MARMARA UNIVERSITY
INSTITUTE FOR GRADUATE STUDIES
IN PURE AND APPLIED SCIENCES

AUTOMATED FITTING PROCESS TO ESTIMATE THE PARAMETERS OF MICROCYLINDER APPEARANCE MODEL BASED ON PHOTOGRAPHS

CİHAN BAL

MASTER THESIS

Department of Computer Science and Engineering

Thesis Supervisor

Asst. Prof. Dr. Mehmet Kadir Baran

ISTANBUL, 2020

MARMARA UNIVERSITY
INSTITUTE FOR GRADUATE STUDIES
IN PURE AND APPLIED SCIENCES

AUTOMATED FITTING PROCESS TO ESTIMATE THE PARAMETERS OF MICROCYLINDER APPEARANCE MODEL BASED ON PHOTOGRAPHS

CİHAN BAL

(524115024)

MASTER THESIS

Department of Computer Science and Engineering

Thesis Supervisor

Asst. Prof. Dr. Mehmet Kadir Baran

ISTANBUL, 2020

MARMARA UNIVERSITY
INSTITUTE FOR GRADUATE STUDIES IN PURE AND APPLIED SCIENCES

Cihan Bal, a Master of Science student of Marmara University Institute for Graduate Studies in Pure and Applied Sciences, defended his thesis entitled **"Automated Fitting Process To Estimate the Parameters Of Microcylinder Appearance Model Based On Photographs"**, on Feb 03, 2020 and has been found to be satisfactory by the jury members.

Jury Members

Assist.Prof. Mehet K. BARAN (Advisor)
Marmara University, Department of Computer Engineering ....

Prof.Dr. Çiğdem EROĞLU ERDEM (Jury Member)
Marmara Üniversitesi, Department of Computer Engineering ....

Assist.Prof. S. Murat YEŞİLOĞLU (Jury Member)
İstanbul Technical University Department of Control and Automation Engineering ....

APPROVAL

Marmara University Institute for Graduate Studies in Pure and Applied Sciences Executive Committee approves that Cihan Bal be granted the degree of Master of Science in Department of Computer Engineering, Computer Engineering Program on ....05.02.2020.... (Resolution no:....2020/05-02.......).

Director of the Institute Prof.
Prof. Dr. BÜLENT EKİCİ

ACKNOWLEDGMENT

A great time, effort, passion has been put into this thesis.
Special thanks for everybody who contributed to making this thesis possible.

11.2019 **CİHAN BAL**

TABLE OF CONTENTS

ABSTRACT

AUTOMATED FITTING PROCESSES TO ESTIMATE THE PARAMETERS OF MICROCYLINDER APPEARANCE MODEL BASED ON PHOTOGRAPHS

Rendering high quality woven fabric images, especially transparent fabrics like curtains, need special rendering techniques that differ from standard approaches. Since a woven fabric consists of vertically and horizontally crossing elliptical yarns and yarns, consist of cylindrical microfibers, a suitable, revised rendering approach is needed. Therefore, a rendering model for woven fabric images is proposed “Microcylinder Appearance Model”. In this thesis, the microcylinder appearance model is examined in detail. This model is one of the most famous works in the computer graphics community that applies to real-time rendering scenarios. The model needs some parameters to produce a realistic rendering of different fabric types such as silk, linen, velvet, and polyester satin. In the original article, authors derived these parameters via eye inspection. The purpose of this thesis is to propose a framework that attempts to extract these parameters via image processing techniques.

ÖZET

MİKRO SİLİNDİR GÖRÜNTÜ MODELİNİN PARAMETRELERİNİN FOTOĞRAFTAN ÇIKARILMASI

Kumaşların yüksek kalite görüntülerinin oluşturulması, özellikle de tül gibi transparan kumaşların görüntülerinin oluşturulması için var olan diğer yaklaşımlardan daha farklı bir yaklaşımın benimsenmesi gerekmektedir. Dokuma kumaşlar birbirlerini dik kesen elips gibi ipliklerden oluşur ve bu ipliklerde silindirik microfiber yapıların bir araya getirilmesinden oluşmuştur. Bu yapıya özel yenilenmiş bir görüntüleme algoritmasına ihtiyaç vardır. Bu sebeple dokuma kumaşların görüntülenmesi için özel bir model geliştirilmiştir. "Mikro Silindir Görünüm Modeli" Bu tezde mikro silindir görüntü modeli detaylı bir şekilde incelenmiştir. Bu model bilgisayar grafikleri alanında, gerçek zamanlı görüntü oluşturmaya yatkın en popüler modellerden biridir. İpek, keten, kadife ve polyester saten gibi farklı türlerin görüntülerini oluşturabilmek için bu modelin parametrelerinin belirlenmesi gerekir. Bu modelin anlatıldığı makalede yazarlar parametreleri kumaşların göz ile inceleyip ilgili parametreleri belirlemişlerdir. Bu tezin amacı model için gerekli parametreleri imaj işleme yöntemleri ile otomatik olarak çıkaracak bir sistem geliştirmektir.

SYMBOLS

$\Psi_{diffuse}$	: Diffuse component of Kajiya-Kay's lighting model.
k_d	: Diffuse multiplier.
k_s	: Specular multiplier.
$\Psi_{specular}$	: Specular component of Kajiya-Kay's lighting model.
Ψ_{hair}	: Goldman's hair model.
ω	: Solid angle.
Lo	: Outgoing radiance.
L_i	: Incident radiance.
L_r	: Reflected radiance.
ω_{eye}	: Looking direction.
$\omega_{incident}$	: Light direction.
ω_r	: Reflection direction.
θ	: Longitudinal angle.
t	: Tangent direction.
γ_s	: Surface roughness.
γ_t	: Tangent deviation.
η	: Refraction index.
n	: Surface normal.
σ	: Standard deviation.
μ	: Mean.
α	: Ratio.
A	: Albedo.

ABBREVIATIONS

MAP	: Microcylinder Appearance Model
BRDF	: Bidirectional Reflectance Distribution Function
BSDF	: Bidirectional Scattering Distribution Function
DFT	: Discrete Fourier Transform
FCM	: Fuzzy C Means Clustering
PCA	: Principal component analysis
SVM	: Support Vector Machine
CVN	: Convolutional Neural Network

LIST OF FIGURES **PAGES**

LIST OF TABLES **PAGES**

CHAPTER 1 – INTRODUCTION

1.1 Problem definition

The main goal of this thesis is to discuss the ways to extract parameters of a particular shading model "Microcylinder Appearance Model" (MAP) from a single photograph of fabric using image processing techniques.

MAP is a specific model that is crafted for the rendering of woven fabrics. It includes several parameters which are mostly based on the fabric's weaving pattern and characteristics of the yarn used in the fabric. Such as yarn colors, microfiber density in the yarn, the construction method of the yarn, i.e. twisting or gluing microfibers together. Finally, and most importantly, the smallest patch which can construct fabric pattern when consecutively repeated.

There will be a proposition of a robust pipeline that includes fabric image acquisition, segmentation "See Fig 1.1" and estimation of waving pattern. "See Fig 1.2" This pipeline can be used to acquire MAP parameters in future work.

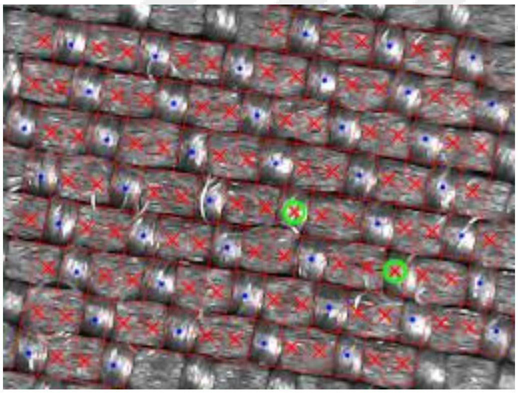

Figure 1.1 Segmented and classified fabric image.

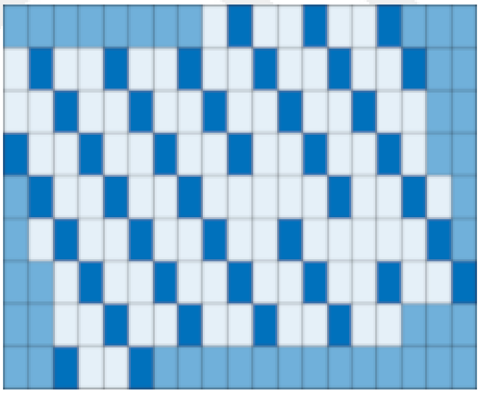

Figure 1.2 Estimated weaving pattern.

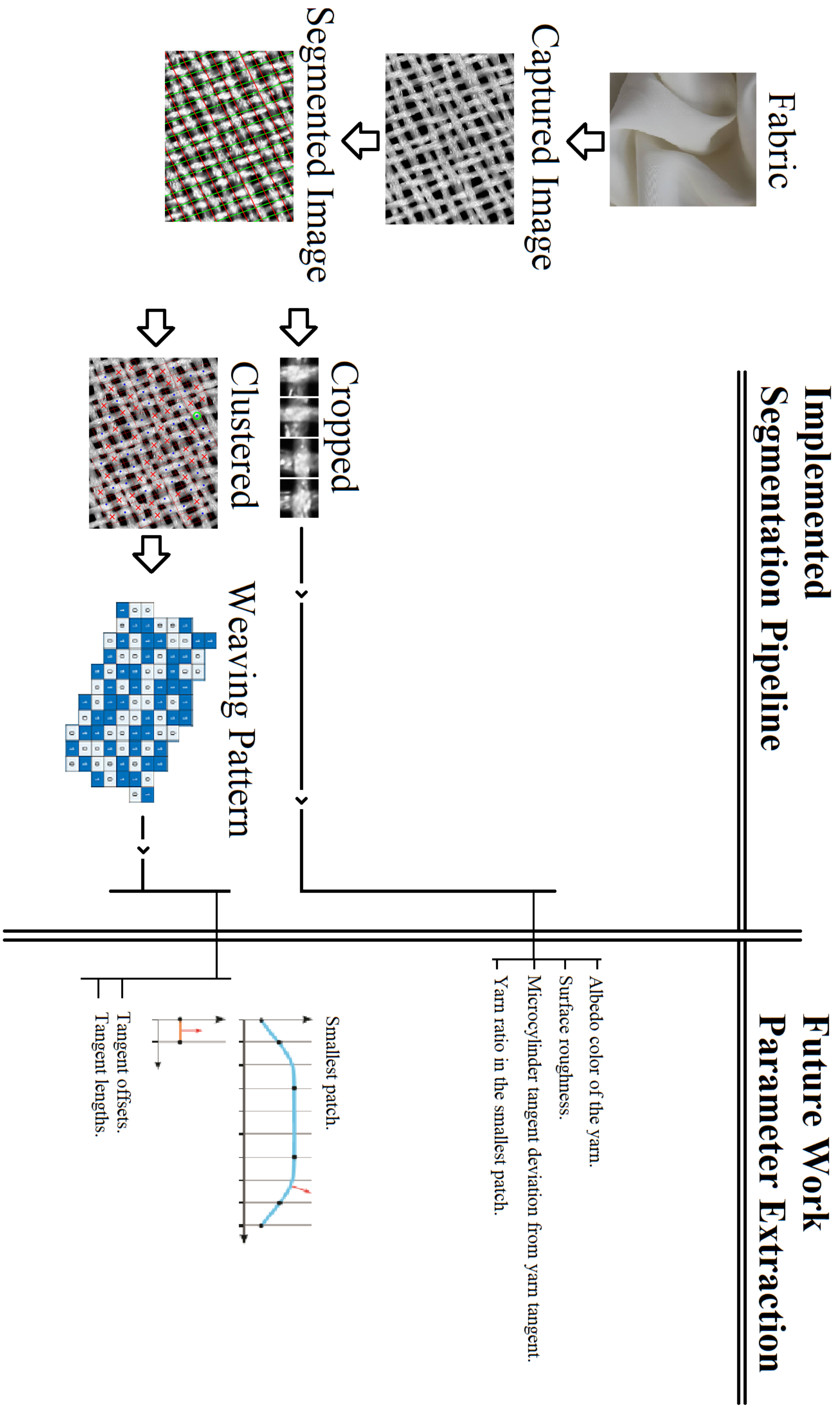

Figure 1.A Information flow from segmentation to parameter extraction.

1.2 Previous Works

3d graphics and image processing fields needed to be researched to achieve the goal of this thesis, that is why it is appropriate to divide this section into two sub-sections. In the first part of this section, the previous works that lead to the MAP model are examined, and for the last part, we will see various attempts that have made to segment and classify basic woven fabric images.

1.2.1 Rendering

Achieved appealing fabric renders have an extensive research background. Since fabrics are made of yarns and yarns are constructed from microfibers, it is expected them to behave like hair. So, it would be appropriate to get inspired by hair shading models. MAP model is indeed inspired by Marchener et al. “Light Scattering from Human Hair Fibers” [1], along with many others’ research. To understand how different light behaves when it is exposed to a cylindrical shape, we should get back to one of the very first research that has made by Kajiya and Kay. [2] They described a Bidirectional Reflectance Distribution Function (BRDF) specifically designed to simulate light beams scattering through cylinders. “fig 1.3” They calculated the diffuse reflected light from the cylindrical surface by integrating Lambert’s model around a semi-circle.

$$\Psi_{diffuse} = k_d \int_0^{\pi} l.nrd\theta$$

$$= k_d r \int_0^{\pi} l\big(b(\cos(\theta)) + l'(\sin(\theta))\big)d\theta$$

$$= k_d r l' \int_0^{\pi} \sin(\theta)\, d\theta$$

$$= (K_d) l.l'$$

Diffuse lighting calculation for Kajiya-Kay’s model. (1.1a)

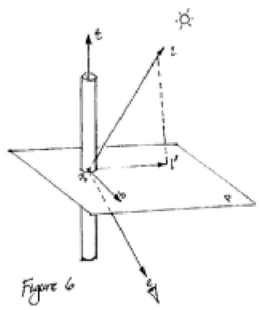

Figure 1.3 Kajiya-Kay’s model construction. Figure reference [2]

To incorporate specular lighting, they used an ad hoc model like Phong specular model. They have shown that light hitting a cylindrical surface will scatter within a cone “fig 1.4”, and the closer the eye to the cone surface, the brighter the highlights will be as analogues to Phong specular model.

$$\psi_{specular} = k_s \cos^p(e, e')$$

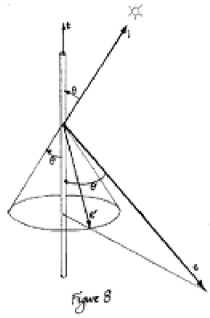

Specular lighting calculation for Kajiya-Kay’s model. (1.1b)

Figure 1.4 Kajiya-Kay’s specular reflection cone. Figure reference [2]

Rendering results and GLSL shader implementation of the model is stored in a public repository. [35].

Goldman has improved this model in his paper “Fake Fur Rendering” [3] He catches that the light that hits the furry animals from behind seems brighter than front light and proposes an ad hoc method to capture this effect. He proposed a directional attenuation factor by including transmitted light and reflected light factors in Kajiya-Kay’s BRDF.

$$f_{dir} = \frac{1+K}{2}\rho_{reflect} + \frac{1-K}{2}\rho_{transmit}$$
$$\psi_{hair} = f_{dir} f_{surface}\left(\psi_{diffuse} + \psi_{specular}\right)$$

Goldman’s modified hair shading model. (1.2)

Kim took Goldman’s directional attenuation idea and placed it on a more physically correct basis in his Ph.D. thesis. [4] He divided surface reflection into two parts; longitudinal part, which is along the tangent direction and azimuthal part, which is along the circumference of the hair tangent. He proposed that the reflected light is not equally distributed around reflection cone, but it behaves differently based on the viewing direction. Like what Goldman says. However, he assumed the hair fiber as a perfect mirror and calculated reflection from the surface and polar plot the energy reflection "See Fig 1.5" from the same side of the light.

$$R(\phi') = \begin{Bmatrix} I\rho_r \cos(\phi'/2), -\pi \leq \phi' \leq \pi \\ 0, otherwise \end{Bmatrix}$$

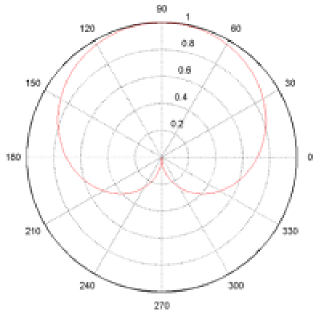

Kim's backward scattering attenuation factor. (1.3)

Figure 1.5 Backward scattering energy plot. Figure reference [4]

Kim also applied the same idea to transmitted light from the hair fiber "fig 1.6" and stated that due to refraction, the transmitted light is much narrower and stronger compared to forward scattering.

$$T(\phi') = \begin{Bmatrix} I\rho_t \cos\big(k(\phi' - \pi)\big), |\phi'| \geq \pi\left(1 - \frac{1}{2k}\right) \\ 0, otherwise \end{Bmatrix}$$

Kim's forward scattering attenuation factor. (1.4)

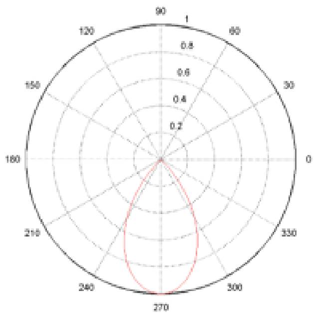

Figure 1.6 Forward scattering energy plot. Figure reference [4]

Finally, to produce the final Bidirectional Scattering Distribution Function (BSDF), Kim combined the reflectance and transmittance attenuation factors “See Fig 1.7” and multiply it by Kajiya-Kay’s BRDF function.

$\psi_{hair} = (\psi_{diffuse} + \psi_{specular})(\rho_r R(\phi') + \rho_t T(\phi'))$ Kim’s attenuated BRDF model. (1.5)

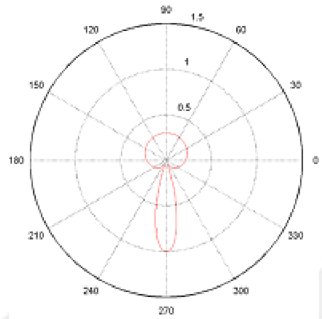

Figure 1.7 Combined attenuation functions. $\rho_r = 5, \rho_t = 1.0, k = 5.0$ Figure reference [4]

Rendering results and GLSL shader implementation of the model is stored in a public repository. [36].

Lastly but not least importantly, Marschner et al. should be mentioned with their work on “Light Scattering from Human Hair Fibers”. [1] MAP is very similarly constructed, as explained in their article. Measurements and scattering geometry, along with azimuthal and longitudinal scattering functions, will be discussed briefly here. Their scattering scheme is the most detailed one that will be explained throughout this thesis, and most of the concepts will be briefly explained. It is appropriate to start with modes of reflection across a cylindrical interface. They use the terms T for transmittance and R for reflectance. They considered three modes of reflection. R for reflection from the fiber surface. TT for transmitting through fiber and TRT for internal reflections. “See Fig 1.8”

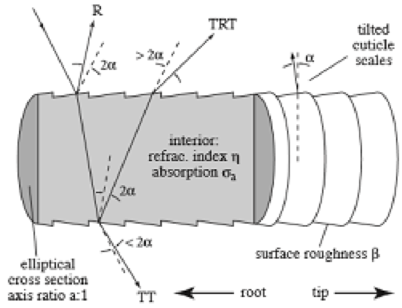

Figure 1.8 A schematic model for a hair fiber. Figure reference [1]

They measured light reflection from a 2d cross-section of the full 3d BSDF, which is captured via a gonioreflectometer. Consider a hair fiber that is hanged root to tip and let stay in its natural form and a camera making -60 degrees with fiber normal along with a light source making 15 degrees with fiber's normal coplanar to camera. Then capture the image and move the light source. By moving the light source and measuring intensities of the captured images, they were able to measure light scattering from hair fibers. "See Fig 1.9"

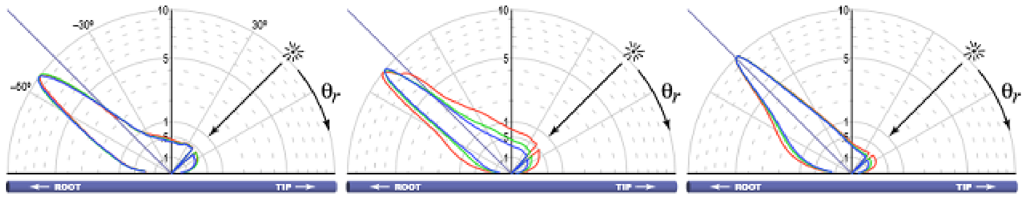

Figure 1.9 Scattering measurements from different hairs. From left to right. Black, blond, synthetic hairs. Figure reference [4]

In order to calculate refraction over the 2d cross-section of a cylinder, they used the Bravais index, which project incident light on the plane that perpendicular to fiber tangent and changes refraction indexes accordingly. "See Fig 1.10" Calculation of longitudinal scattering is straight forward. Rough surface and existence of cuticle scales shifts longitudinal scatters randomly away from the ideal reflection cone.

$$M_R(\theta_h) = g(\beta_r; \theta_h - \alpha_R)$$
$$M_{TT}(\theta_h) = g(\beta_{TT}; \theta_h - \alpha_{TT})$$
$$M_{TRT}(\theta_h) = g(\beta_{TRT}; \theta_h - \alpha_{TRT})$$

Longitudinal scattering functions, where “g” is normalized Gaussian function. (1.6)

However, azimuthal scattering is a bit more involved and can be examined from “See Fig 1.10”. Paths for R, TT and TRT must be found by solving this equation:

$$\phi(p, h) = 2p\gamma_t - 2p\gamma_i + p\pi \tag{1.7}$$

Where p is the internal path segments. It encompasses all three scattering modes.

R if p=0,

TT if p = 1

TRT if p = 2

Therefore, azimuthal scattering function is $N(\phi) = \sum_p N_p(p, \phi)$ (1.8)

$$S(\phi_i, \theta_i; \phi_r, \theta_r) =$$
$$M_R(\theta_h) N_R\,(\eta'(\eta, \theta_d); \phi)/\cos^2(\theta_d) +$$
$$M_{TT}(\theta_h) N_{TT}\,(\eta'(\eta, \theta_d); \phi)/\cos^2(\theta_d) +$$
$$M_{TRT}(\theta_h) N_{TRT}\,(\eta'(\eta''(\phi_h), \theta_d); \phi)/\cos^2(\theta_d)$$

Complete scattering function. (1.7)

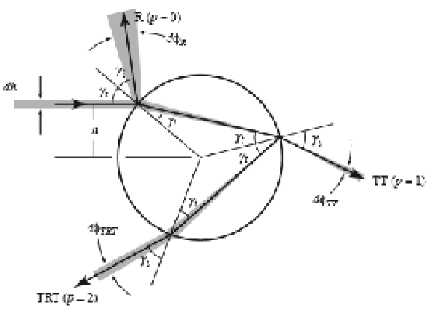

Figure 1.10 Scattering from a circular cross-section. Figure reference [4]

This section can be concluded. All the previous significant works have been mentioned here, and other topics related to rendering and shading of MAP will be introduced in a chapter dedicated to it. “2.1.3 Micro cylinder appearance model”.

1.2.2 Image processing

In this part of the thesis, previous related works will be examined. Works are categorized by relevance to the proposed solution in this thesis rather than chronological order.

One of the first problems that have been encountered was to axis align weft and warp yarns in the captured image to further process the image. Guarnera et al. proposed an approach using radon transform in their “Woven Fabric Model Creation from a Single Image” article. [5] A similar technique is used in this thesis, so it is worth to mention them here. The interesting part of their pipeline in terms of our needs will be outlined and explained shortly. To segment a fabric image and extract repeating pattern, they suggest four steps pipeline.

1. Data Capture: Acquire an image of the textile product.
2. Initial Image Processing: Axis align the yarns in the image and create Fourier Signature for a database lookup.
3. In-homogeneous and Homogeneous Fabric Analysis: Extract fabric pattern and save it in the database to look it up later.
4. Depth Map Creation: For rendering high detailed realistic fabric images.

One of the interesting parts of their work is that they assumed the image to be a linear combination of three different signals. $F(I) = F(I_r + I_l + I_n) = F(I_r) + F(I_l) + F(I_n)$ (1.8) Where the first term assumed to be a perfectly woven fabric weaved with a perfect loom machine and the image considered to be captured with a perfect camera. However, in real life, there are irregularities caused by the loom machine and noise caused by dust and lint. With the aid of linearity of Discrete Fourier Transform (DFT) separating the I_r to process further is possible. In probabilistic terms, if a big enough fabric sample can be captured, the probability of seeing I_r is significantly higher than seeing the deformations due to loom machine imperfection or dust captured by the camera.

For our purpose, the most interesting part is the way they extract yarn alignments. To find the dominant inclination caused by the yarns, they suggested applying radon transform to log-magnitude of the DFT of the image. Because the yarns are periodically repeating themselves, they expected to see bright peaks in the radon space, which points out significant inclination.

$$RT_{s,\phi} = \iint_{-\infty}^{\infty} f(x,y)\delta(x\cos\phi + y\sin\phi - s)dxdy$$

Radon transform. (1.9)

$$\tau_I = \int \left|RT_{s,\phi}\big(\log F(I_r + I_l)\big)\right| ds$$

Radon transform of log-magnitude of Fourier transform of the image. (1.10)

$$\alpha = argmax \frac{d\sigma_\phi}{d\phi}$$

Peak search function in radon space. (1.11)

Another approach worth mentioning is using autocorrelation to find repeating unit sizes. Kang et al. used autocorrelation across the width and height of the image to find repeating structure sizes in the image. [6] "See Fig 1.12" Since it is expected in a basic weaving pattern to repeat itself with simple units, this approach produces good results with basic patterns such as plain weaving.

$$C_{x,0} = \sum_{i}^{M}\sum_{j}^{N} G_{i,j}G_{i-x,j}$$

$$C_{0,y} = \sum_{i}^{M}\sum_{j}^{N} G_{i,j}\,G_{i,j-y}$$

Autocorrelation along the axis-aligned yarn directions. (1.12)

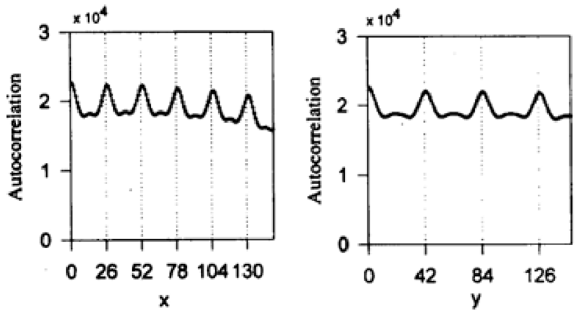

Figure 1.12 Autocorrelation plots along the width and height of the image. Figure reference [6]

Schröder et al. made a significant contribution when it comes to extracting out the minimal repeating unit from the fabric sample in their article “Image-Based Reverse Engineering and Visual Prototyping of Woven Cloth”. [7] They first apply autocorrelation to find the size and locations of the repeating unit as Kang et al. However, they further apply flow fields to fix the structural deformation in the whole image and extract the regular image to apply segmentation successfully. They come up with the idea of “Regularized Median Image”. “See Fig 1.13” They construct this image by averaging up the cut-out sub-images found by autocorrelation. In this way, the boundaries of each yarn become much more visible, which helps the segmentation. Then they place the median image against one of the repeating units and applied optical flow [8] to estimate the displacement of each pixel up against the mean image. Also, they applied a regularization factor while finding the displacement. Bigger regularization factors correspond to deformation of the whole image, coarse flow, and smaller regularization factors correspond to yarn level deformations that they called fine flow. “See Fig 2.11”

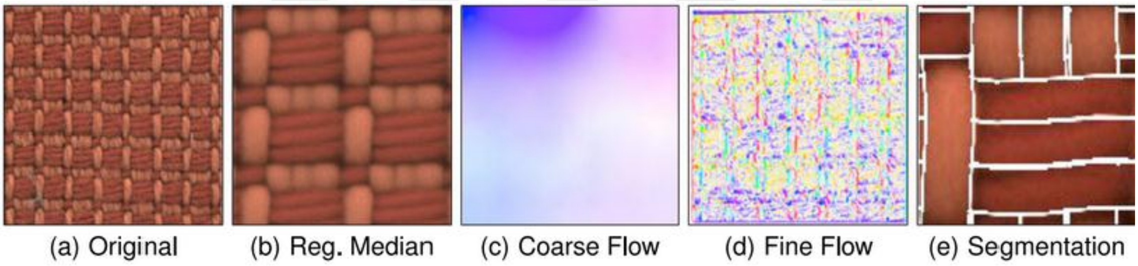

Figure 1.13 Segmentation process. Figure reference [7]

Another significant contribution has been made by Kuo at al. with their work “Automatic Recognition of Fabric Weave Patterns by a Fuzzy C-Means Clustering Method”.[9] They have come up with the idea of projection profiles along with the width and height of the image to find boundaries of each yarn “See Fig 1.14” and segmented the image using found boundaries. They used first-order statistics (mean and standard deviation) and second-order statistics (contrast and homogeneity of co-occurrence matrix with distance, 1 and 90 degrees) [10] to divide the segmented regions into two clusters, weft and wrap clusters using fuzzy c means clustering. (FCM) “See Fig 1.15”.

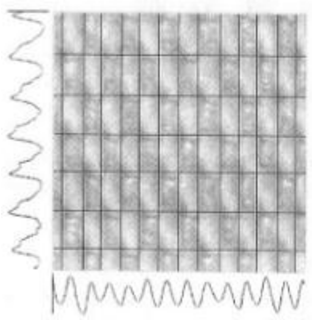

Figure 1.14 Projection profiles along width and height. Figure reference [9]

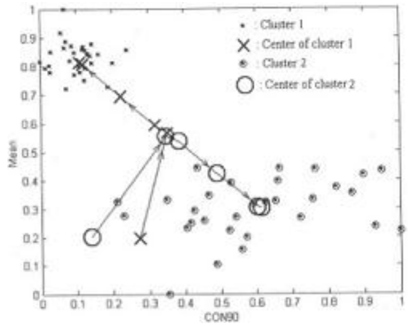

Figure 1.15 Clustering plots. Figure reference [9]

$$J_{FCM} = \sum_{i=1}^{c} \sum_{j=1}^{n} u_{ij}^{m} d_{ij}^{2}$$

$$u_{ij} \in [0,1], d_{ij} = [\![w_i - x_j]\!]$$

Fuzzy clustering objective function. (1.13)

$$H(y) = \sum_{x=1}^{N} I(x,y)$$

$$V(x) = \sum_{x=1}^{M} I(x,y)$$

Horizontal and vertical projection lines. (1.14)

1.3 Proposed Solution

This thesis aims to propose a parameter extraction pipeline for the MAP model. The most crucial parameter is the smallest patch which can construct the pattern by repeating itself. “See Fig 1.16” Under the light of previous works, a pipeline is constructed to acquire and segment the fabric image. “See Fig 1.17”

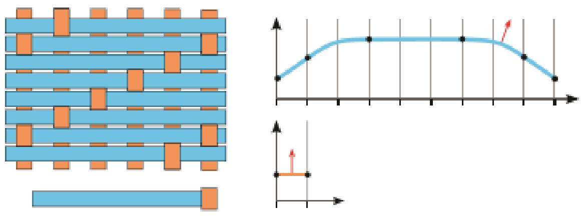

Figure 1.16 Smallest patch of a weaving pattern and patch’s tangent curves. Figure reference [17]

1. Capture the fabric sample on a black background with a USB microscope camera connected to the PC.
2. Enhance the image
   2.1. Apply the Gaussian filter to focus on the regular structures of the sample image.
   2.2. Apply histogram equalization to increase the contrast of the image, which will produce better features for clustering.
3. Find yarn alignments
   3.1. Like radon transform, generate projection histograms from angle 1 to 180 degrees.
   3.2. Normalize the projections by element count in the corresponding bins of the histogram for a fair comparison between each projection profile.
   3.3. Apply low pass filtering to eliminate noise in the projection and emphasize the underlying regular structure.
   3.4. Apply DFT to the projection profile and extract the maximum peak after the DC component.
   3.5. Select the projection profile, which has the highest peak in the frequency space. It both shows the location, count, and alignment of the yarns.
4. Find the yarn crossings.
   4.1. Create a grid at which pass through local minima of the projection profiles.
   4.2. At each intersection of the projection profile, there is a yarn crossing. Apply bilinear mapping to align and fit crossing sub-images in a square of selected size for future processing.
5. Cluster the extracted crossing images.
   5.1. Extract gray-level texture features from the crossing images.
   5.2. Apply Principal Component Analysis (PCA) to reduce redundancy in the feature set.
   5.3. Apply FCM.
6. Estimate the weaving pattern.
   6.1. Ask labels of 4 samples taken from a cluster to identify cluster labels.
   6.2. Generate 0-1 grid to represent weaving pattern
7. Apply autocorrelation to the weaving pattern to find minimal repeating unit

Stage 1 | Stage 2 | Stage 3

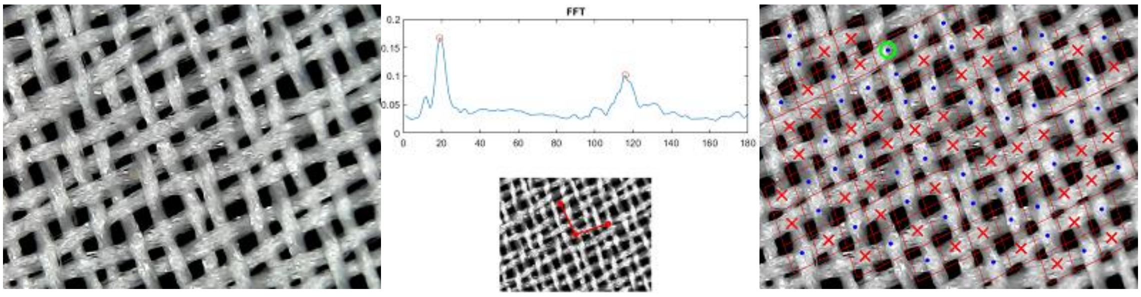

1.1 Acquired image. | 2.1 Yarn alignments detected. | 3.1 Clustered and classified.

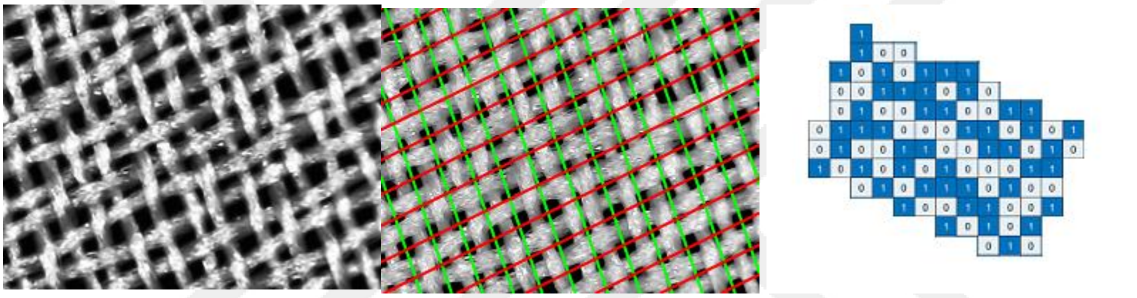

1.2 Enhanced image. | 2.2 Segmented image by yarns. | 3.2 Estimated weaving pattern.

Figure 1.17 Pipeline stages and results.

The proposed pipeline and MAP model will be explained in detail in the next chapter.

CHAPTER 2 – MATERIAL AND METHOD

At the beginning of this chapter, the MAP model will be explained in detail and afterward, the techniques used in the image processing pipeline will be discussed. This pipeline will be used to extract MAP parameters in future works.

As seen in "Fig 1.A" cropped images will be used to collect 4 parameters of the MAP model.

A	Albedo color of the yarn.
k_d	Surface roughness.
γ_s	Microcylinder tangent deviation from yarn tangent.
γ_t	Yarn ratio in the smallest patch.

For the surface roughness and tangent deviation, statistical approaches can be used and for the albedo color and yarn ratio, again image processing techniques can be utilized.

Tangent Offsets	Smallest patch curve definition.
Tangent Lengths	Smallest patch curve definition.

Finally, for the tangent curves, extracted image patterns can be used with autocorrelation to find the smallest patch. These ideas further improved and discussed in chapter 4.

2.1 Micro cylinder appearance model

"A Practical Microcylinder Appearance Model for Cloth Rendering" [17] developed by Sadeghi et al. is the basis for all the work. Assuming the previous chapters provide the necessary background. This chapter builds on top of them. MAP is also a BSDF function that describes how a woven fabric image distributes the incident light from a particular looking direction. It behaves highly anisotropic. The construction of the woven fabric, colors and types of the yarns drastically affects the distribution of light. "See Fig 2.9"

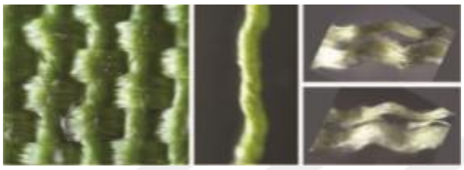

Figure 2.9 "Silk crepe de chine" with individual yarn visuals. Figure reference [17]

In order to match the MAP model with the light distribution of fabrics, some measurements needed to be done. Light distribution of patches investigated using a gonioreflectometer. "Silk crepe de chine" fabric sample examined under a microscope. This fabric sample is made of two distinct yarn types. The first one is straightly moving along the yarn, and it made of densely put together microfibers and twisted together. The second yarn type is perpendicular to the first one and goes below and above of the first yarn horizontally. Also, the yarn is thin and untwisted, exhibiting translucent appearance, and sharp surface highlights. Measurements show strong anisotropic behaviors, so measurements are done from two different alignments which perpendicular to each different yarn types. "See Fig 2.10"

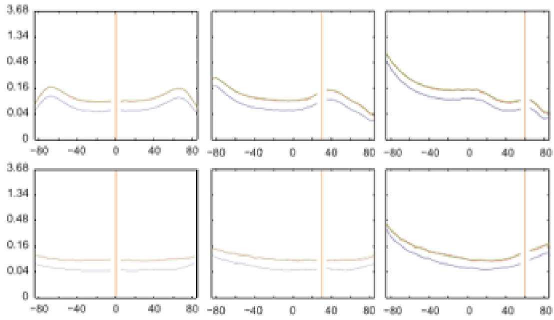

Figure 2.10 BRDF measurements for 0, 30, 60 degrees incident light parallel to flat thread (Top row). Incident light perpendicular to flat thread (Bottom row). Figure reference [17]

The yarn BSDF model is also measured to accompany BRDF measurements from fabric samples and understand the behavior of each yarn. A thread extracted from a sample patch and hanged on the gonioreflectometer's apparatus to measure its full 4D scattering function. "See Fig 2.11" Scattering geometry used in calculation of MAP needed to be addressed here. All the angles are measured against the plane, cutting the tangent of the thread perpendicularly. Longitudinal angles are labeled with "θ", and azimuthal angles are labeled with "φ". Incident vector is denoted with "ϖi", and the reflection vector is denoted with "ϖr" also "t" is the thread tangent and "n" is thread normal. "n" can be arbitrarily chosen when it is not part of a fabric. "See Fig 2.12"

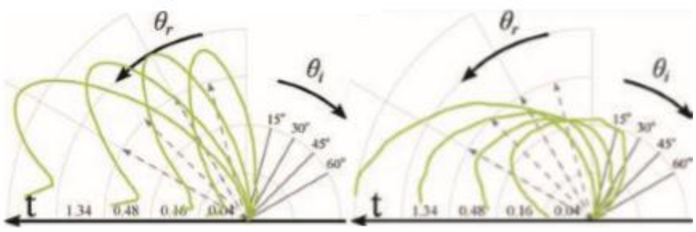

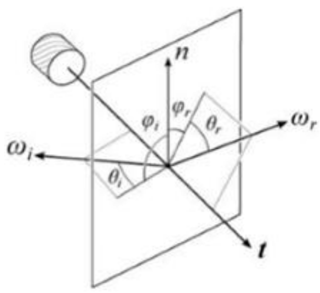

Figure 2.11 Scattering along the thread's tangent. Flat silk on the left. Twisted silk on the right. Figure reference [17]

Figure 2.12 Proposed scattering geometry. Figure reference [17]

It is appropriate to start the discussion of the scattering function from cylinders. Unlike standard irradiance integral on a surface, cylindrical integral on the circumference of a circle used because light hitting on a cylinder rod emits the light in a cone parallel to the rod's tangent. [2]

$$L_r = \int f_s(t, \omega_i, \omega_r) L_i(\omega_i) \cos\theta_i d\omega_i$$

Curve radiance integral from Marschner et al. [1] (2.7)

Here the scattering function $f_s(t, \omega_i, \omega_r)$ is divided into two parts; surface reflection f_{rs} and volume reflection f_{rv} as previously addressed. Hanrahan et al. [18]

$$\phi_d = \phi_i - \phi_r$$
$$\theta_h = (\theta_i + \theta_r)/2$$
$$\theta_d = (\theta_i - \theta_r)/2$$

Accompanying angles introduced to scattering geometry. (2.8)

Surface reflection is $f_{rs}(t, \omega_i, \omega_r) = F_r(\eta, \omega_i)\cos(\phi_d/2) g(\gamma_s, \theta_h)$ (2.9) here the term $\cos(\phi_d/2)$ is due to the projection of the circular cross-section, as stated by Kim. $g(\gamma_s, \theta_h)$ is here to simulate surface roughness. Finally, a Fresnel attenuation factor is added for bringing the model to a physical basis.

Volume reflection is modeled such that microcylinders put together to create a large cylinder. Due to internal reflections occurring between microcylinders, cylinders emit lights to ideal reflection cone the same as the surface reflection. It is assumed that a light beam enters the cylinder goes under any internal reflection and reflected on the ideal reflection cone again.

$$f_{rv}(t, \omega_i, \omega_r) = F \frac{(1 - k_d) g(\gamma_v, \theta_h) + k_d}{\cos\theta_i + \cos\theta_r} A$$
$$F = F_t(\eta, \omega_i) F_t(\eta', \omega_r')$$

Volume reflection function. (2.10)

Two transmission Fresnel terms due to light beam-thread penetration are modeled with F. Sub cylinder tangent deviations are modeled with a Gaussian blob "g" and refracted light beam absorption is captured by thread albedo color A. Sum of cosine projections is a normalization factor due to multiple scattering in a semi-finite medium defined by Chandrasekar. [19]

$$f_s(t, \omega_i, \omega_r) = (f_{rs}(t, \omega_i, \omega_r) + f_{rv}(t, \omega_i, \omega_r))/\cos^2 \theta_d$$

Total BSDF function for the MAP model. (2.11)

$\cos^2\theta_d$ is introduced by Marchener [1] to account for solid angle attenuation of the specular cone.

Finally, this section can be concluded by giving the full appearance model. This model is constructed such that, in a pixel, on the screen, there are at least two yarns perpendicular to each as in the smallest patch. "See Fig 2.13" This requires the material to be viewed from a distance, not up close such that individual yarns are visible. The outgoing radiance from a pixel is calculated by iterating the microcylinder model over the smallest patch with random "N" samples for both patches.

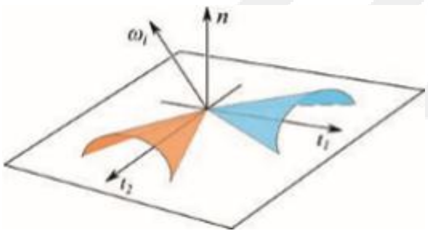

$$L_r(\omega_r) = \alpha_1 \times L_{r,1}(\omega_r) + \alpha_2 \times L_{r,2}(\omega_r)$$

Figure 2.13 Crossing yarns. Figure reference [17]

Outgoing radiance. α is the coverage ratio of each yarn in the smallest patch. (2.12)

Finally, calculated outgoing radiance is averaged for each yarn to complete the full MAP model.

$$L_r, j(\omega_r) = \frac{1}{N_j} \sum_t \int L_i\,(\omega_i) f_s(t, \omega_i, \omega_r) \cos\theta_i d\omega_i \qquad (2.13)$$

The complete MAP function; Sum of individual cylindrical BSDF function for each thread.

Results of the implementation of MAP model "See Fig 2.14" along with the comparison with measurements "See Fig 2.15" and implementation of the author. "See Fig 2.16"

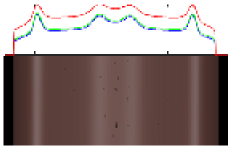

Figure 2.14

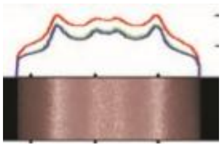

Figure 2.15 Figure reference [17]

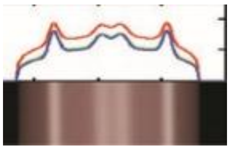

Figure 2.16 Figure reference [17]

GLSL implementation of the MAP model is stored in a public repository. [37].

2.2 Image Processing Techniques

This part consists of efforts made to segment the captured image of a fabric sample and derive the weaving pattern out of it. Each header is given in chronological order in the pipeline and explained in detail with the reasons for the step, inputs, and outputs of the process.

2.2.1 Image acquisition

A USB microscope camera is used to capture the magnified images of the fabric for catching the individual yarns in the fabric sample. It has 1000X magnifying capacity and 2MP digital camera. "See Fig 2.17" It has an adjustable focus length and evenly distributed, brightness adjustable led lights on it. A full black and rough background is used to minimize bright reflections from the background and led lights' brightness adjusted to capture maximum detail. "See Fig 2.18"

Figure 2.17 USB microscope camera.

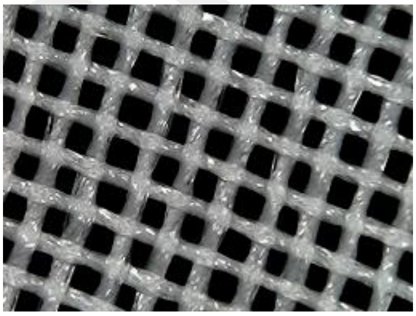

Figure 2.18 Captured sample fabric.

2.2.2 Histogram equalization

A gray level histogram is the distribution of pixel intensities to discrete size bins. For example, a gray image with levels between 0…1 can be fit into eight different bins 1...8. It gives us information about brightness and contrast. For example, a darker image tends to accumulate on the left side of the histogram. The purpose is here to create a flatly distributed histogram to increase contrast in the image. A high contrast image brings more abundant information compared to a low contrast image and produces better textural features for clustering. A technique called histogram equalization is applied to achieve flatly distributed histograms. [20] This enhancement technique gets applied globally. That is, the whole image's light distribution is altered. In our case, the desired effect is to enhance details in the small areas of the image. So, this equalization is applied to small patches in the image instead of applying it globally. This method is called “Adaptive Histogram Equalization”. [21]

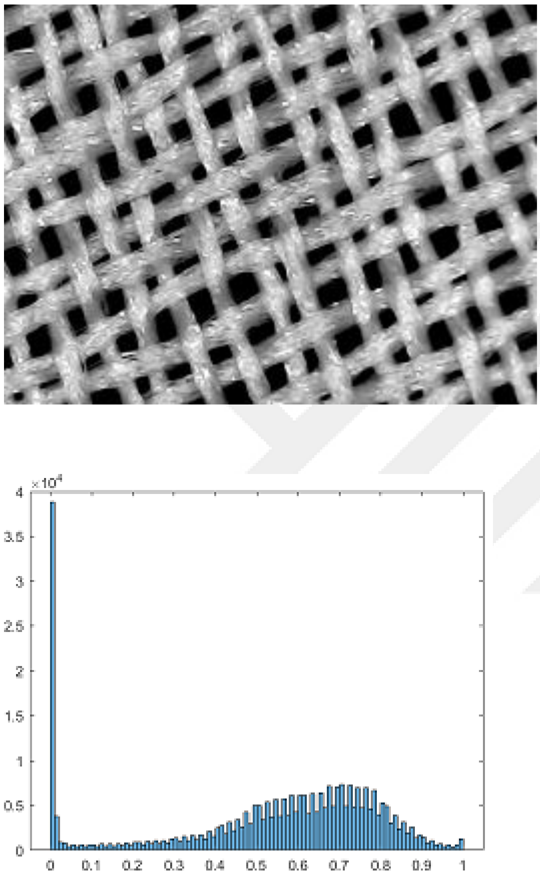

Figure 2.19 Histogram of the captured image.

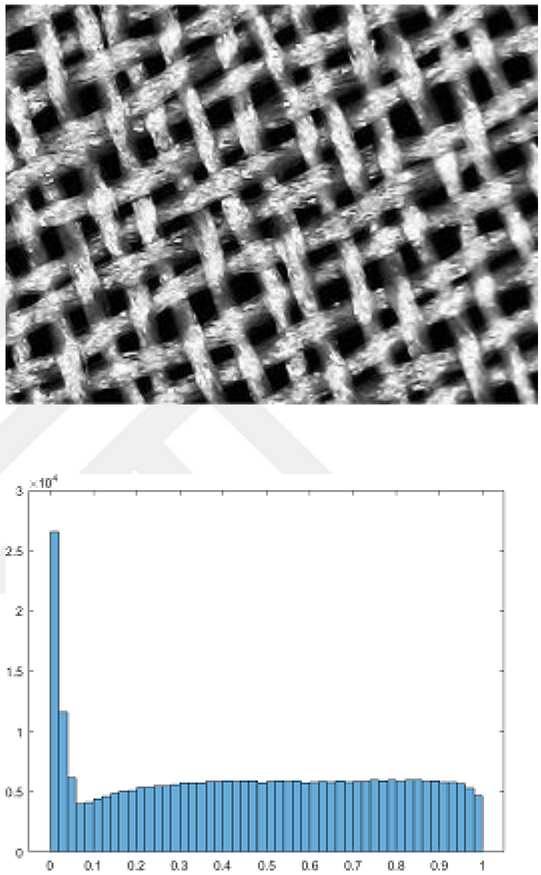

Figure 2.20 Adaptive histogram equalization results.

2.2.3 Gaussian blur

Captured image data needs to be smoothed before applying segmentation algorithms. There might be noise due to dust and high-frequency intensity changes due to irregularities in the yarns. A Gaussian filter of size $2 \times ceil(2 \times \sigma) + 1$ with standard deviation "σ" convolved with the image in the frequency domain.

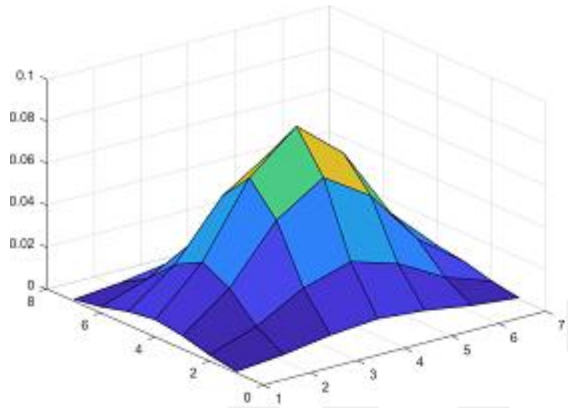

Figure 2.22 Gaussian filter size of 7 with σ 1.14.

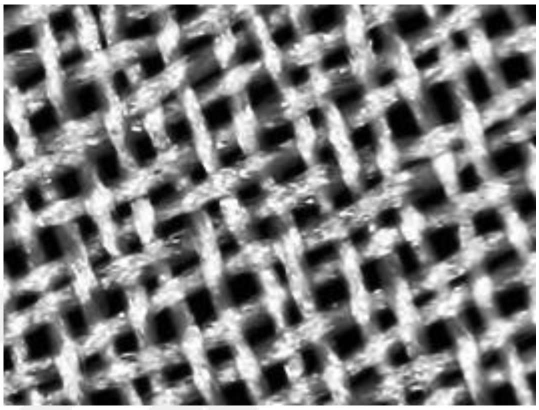

Figure 2.23 Blurred and histogram equalized image ready to process further in the pipeline.

2.2.4 Normalized projection profiles

This phase in the pipeline is critical in order to correctly capture the yarn alignments. Yarn counts and estimated positions will be extracted from this profile. An approach like the radon transform is utilized. The image is projected to the horizontal axis, and each bin that corresponds to an image column is normalized with the number of elements in it. Normalization creates a histogram of averaged pixels. "See Fig 2.24" The high-frequency details are further smoothed out by applying a low pass filter to the profile. Through the investigation on many different fabric images, it is observed that, while projection angle gets close to the alignment of the yarns, profiles start shaping like sinusoids. "See Fig 2.25" To exploit this information, DFT applied to the profile and highest peak after the DC component extracted (stored in "ampMax" to reference in pseudocode). The more a signal like a sinusoid, the higher its amplitude in the frequency domain. At the end of a full spinning of the image from 1 degree to 180 degrees, all gathered amplitudes compared, and yarn alignments are determined according to the given pseudocode below.

Pseudocode:

1. Rotate the image from **i** = 1 degree to 180 degrees.
    1.1. **For Each Degree i** project the pixels on to the horizontal line and create a projection profile consist of bins that contain the sum of projected pixels.
    1.2. Normalize the projection profile by dividing the number of pixels in the bin to the bin's value. In short, this is an averaged projection profile.
    1.3. Apply low-pass filter to hold down the noise in the projections.
    1.4. Apply DFT to the projection profile. In frequency domain take the highest amplitude after the DC component and put it into "ampMax[**i**]".
2. Take the highest value $\mathbf{h_1}$ in "ampMax" and seek a second peak within ($\mathbf{h_1}$ + 90) ± 5 degrees proximity to the first peak.
    2.1. **IF** a secondary peak found within the range, **Return** the first and second degrees and **Success**.
    2.2. **Else IF** no secondary peak found, search for a next candidate peak in the "ampMax" array after the $\mathbf{h_1}$'th peak.
    2.3. **IF** there exists another candidate peak, **Continue** from step 2 **Else Fail**

Example:

After rotating the input image, creating projections and constructing the "ampMax" array; Assume a peak found on the 10'th degree in "ampMax", the algorithm looks for a secondary peak in the range 95-105 degrees. Consider no secondary peak found. Algorithm fallbacks to step 2. Assume it founds another candidate at 40'th degree, the algorithm looks for a secondary peak in the range 125-135 degrees. If it can find a secondary peak, It successes, otherwise the algorithm repeats these steps until no peak remains.

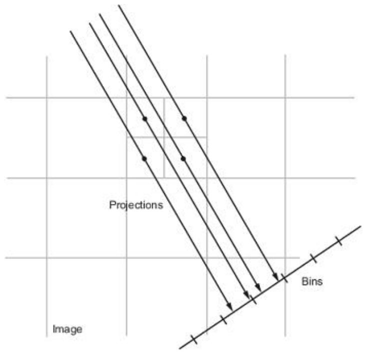

Figure 2.24 Averaged histograms created from projection profiles. Figure reference [31]

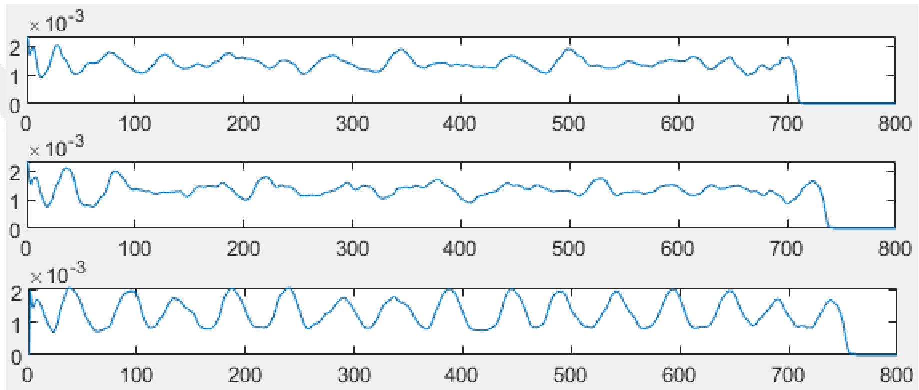

Figure 2.25 Projection profiles getting closer and closer to a sinusoid.

If algorithm success two peaks show the yarn alignments nearly perpendicular to each other. “See Fig 2.26” This algorithm allows detecting alignments of sheared images by up to 10 degrees. Increasing this ± 5 degrees delta might help to capture more sheared images. However, it increases the chance to select wrong secondary angles, which leads to poor segmentation of the image.

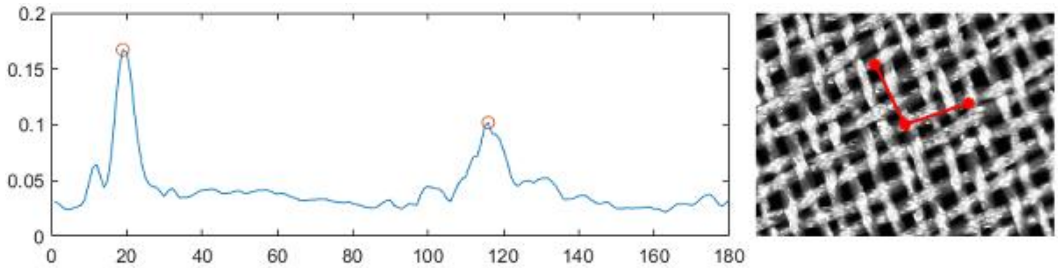

Figure 2.26 Detected peaks in “ampMax”.

2.2.5 Low pass filtering

Projection profiles contain high-frequency noise due to loom machine and capture device imperfections. Summing pixels emphasize these irregularities. The probability of seeing repeating structure regularly in a weaving fabric sample is higher in probabilistic terms, and this regular structure is dominant in low frequencies. [5] Applying a low pass filter in the frequency domain highly reduces these irregularities. Unlike the Gaussian filter that applied to the image, this low-pass filter is applied to the projection profiles and smooth the high-frequency noise in the projections.

2.2.6 Analysis of projection profiles

By analyzing the projection profile, several important information can be generated. The projection profile is mostly processed in the frequency domain, such as low pass filtering and extracting the maximum amplitude. One of the useful information about the peaks found in the frequency domain is that the maximum peak's frequency is equal to the number of yarns visible in that orientation, and the area under the peak shows the visibility status of each yarn in the image. Also, lastly, and most importantly, each local minimum at the projection profile shows the boundaries of each yarn. The intersection of these profiles produces the grid that captures crossing points of yarns "See Fig 2.27" which is vital to extract weaving patterns.

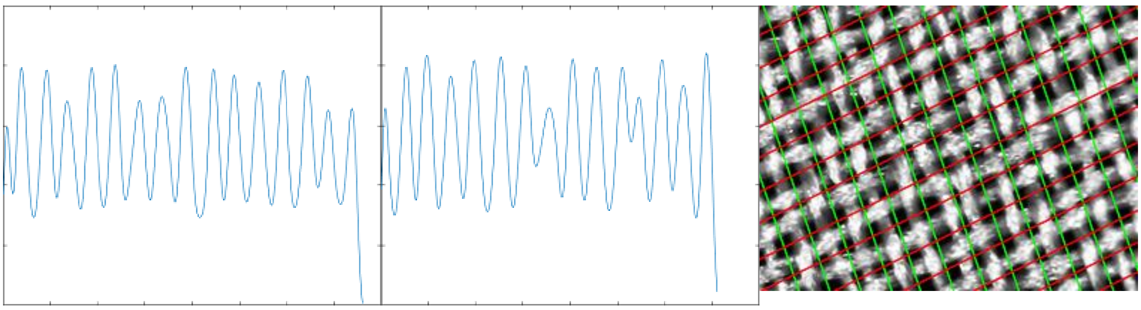

Vertical projections. Horizontal projections. Crossing grid.

Figure 2.27

2.2.7 Bilinear transform

Each extracted intersection will be further analyzed in the next phase of the pipeline. It is essential to compare the crossings images fairly. So, crossings are put into equal size aligned boxes which fixes their orientation and allows to produce the same number of texture features with similar orientations. "See Fig 2.29"

Bilinear mapping is mostly used to solve the mapping problem of a rectangle's corners to an arbitrary quadrilateral. Its geometric interpretation is shown below. [22] "See Fig 2.28"

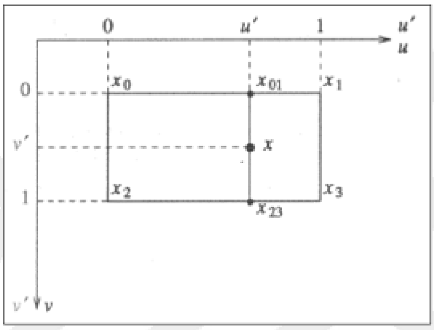

Figure 2.28 Mapping of unit square on to arbitrary quadrilateral.

$$x_{01} = u'(x_1 - x_0)$$
$$x_{23} = u'(x_3 - x_2)$$
$$x = v'(x_{23} - x_{01})$$

Mapping of (u`, v`) to the x. (2.14)

Figure 2.29 Examples of mapped crossings.

2.3 Unsupervised Learning

Up to here, the image is segmented, and crossings at the yarn intersections are extracted. Finally, cropped images are mapped to rectangular fixed-sized images with minimum distortion using bilinear mapping. All the effort is made to extract GLCM features, standardize them for fair comparison, and cluster each crossing into two groups with unknown labels. Two distinct groups label must be figured out. A semi-supervised approach is implemented to assign labels to the clusters. That is, from each one of the clusters, five crossing images are shown to the user and asked to label them. With a majority voting approach, clusters are labeled. For example, if the selected group is voted as “vertical up”, the other group gets labeled “vertical down”. Going full supervised required thousands of crossing samples at hand. Lack of samples left the Support-Vector Machine (SVM) and Convolutional Neural Networks algorithms (CVN) in high bias state, resulting in high prediction errors.

2.3.1 Gray level co-occurrence and texture features

GLCM matrix is constructed by counting the occurrences of pixels with gray levels (i, j) adjacent to each other. This adjacency can be parameterized with directions; Horizontal, vertical and, diagonals. “See Fig 2.30” And distance; Distance of two pixels can be 1, 2, 3 up to image boundaries. In order to make the calculation, the image’s gray level is reduced to “Ng” there for the matrix size is $Ng \times Ng$.

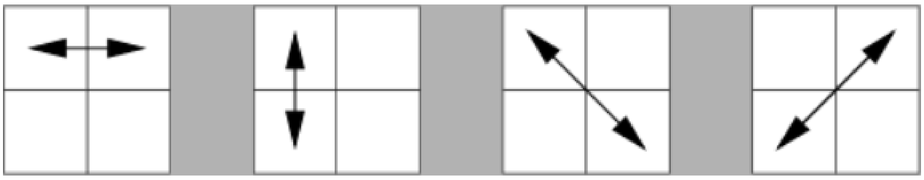

Figure 2.30 Spatial adjacency relations of pixels where the distance is 1. Figure reference [32]

An example matrix is shown below. The image I represent the reduced gray levels of the I. and the GLCM matrix shows counts of each adjacent. For example, adjacent pixels with gray levels (1,1) found once in the image. Therefore, the corresponding matrix entry is one. Pixels with gray levels (1,2) found twice, so the corresponding entry is two and so on. “See Fig 2.31”

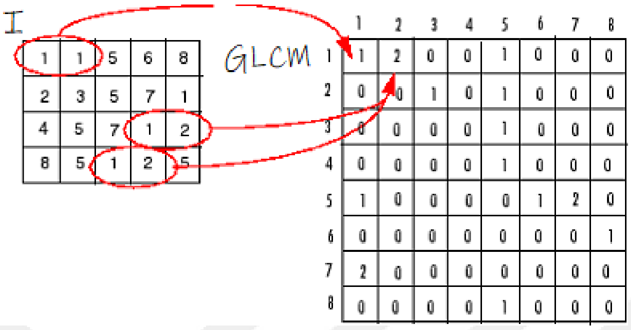

Figure 2.31 Gray level matrix example. Figure reference [34]

By using this matrix, various spatial texture features can be constructed. These features called second-order statistics and successfully used on many classification problems such as analyzing Magnetic resonance images of the brain for Alzheimer disease detection. [23] The features used for clustering the crossing images are given in “table 2.1” with their calculation. [24]

Table 2.1

Contrast	$\sum_{n=0}^{Ng-1} n^2 \{\sum_{i=1}^{Ng}\sum_{j=1}^{Ng} p(i,j)\, p\}, \lvert i-j \rvert = n$
Correlation	$\frac{\sum_i \sum_j (ij)\, p(ij) - \mu_x\mu_y}{\sigma_x\sigma_y}$ $where \mu_x, \mu_y, \sigma_x \text{and} \sigma_y are the means$ $\text{and} std. deviations of p_x \text{and} p_y,$ $the \text{partial} probability density functions.$
Energy	$\sum_i \sum_j p(i,j)^2$
Homogeneity	$\sum_i \sum_j \frac{1}{1+(i-j)^2} p(i,j)$
Entropy	$-\sum_i \sum_j p\,(i,j) \log(p(i,j))$

2.3.2 Feature standardization

Ranges of the features in a vector data vary differently and may reside away from the center of the coordinate system. Many of the comparison algorithms use various distance metrics. For example, in our implementation, FCM uses Euclidean distance to measure the distance of each feature vector for each sample. Some of the features in the vector may take vastly different values from others in scale. This gap causes these features to be more dominant while creating discriminant boundaries and leaving other features unfairly aside. Also, using data with zero means helps to optimize a discriminant function and prerequisite for many machine learning algorithms. For these reasons each feature is normalized “See Fig 2.32”

$\frac{X-\mu}{\sigma}$ Standard score normalization used to normalize each feature. [25]

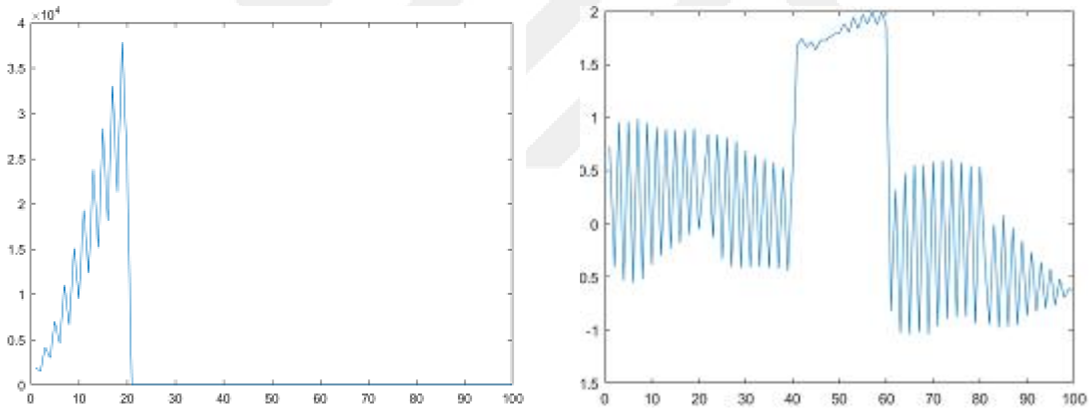

Figure 2.32 Not normalized feature plot is on the left. The normalized version is on the right.

2.3.4 Principal component analysis

GLCM features are characteristically highly correlated, which may cause low performance in clustering. Therefore, reducing the dimensionality of the data is essential. PCA is applied to the feature vector, which consists of 100 features. Reducing the feature count to 8 still preserves 98 percent of the variance in most of the fabric samples. Therefore, dimensionality is reduced by applying PCA to the data. For visualization purposes, data is reduced to 2 dimensions, and two clusters are still clearly separable in "See Fig 2.33".

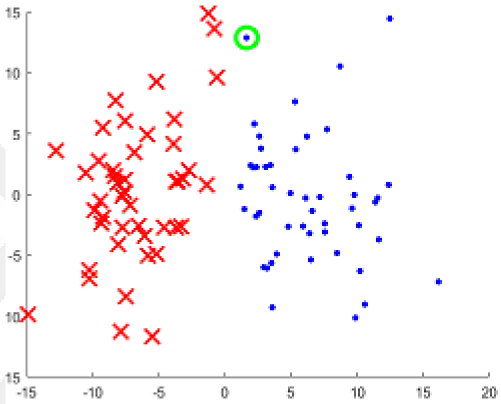

Figure 2.33 PCA applied samples. Green circle points out miss classification.

In many applications, PCA is applied to reduced dimensionality for either reducing storing requirements or processing time for machine learning algorithms. [26] It tries to minimize the projection errors by finding optimal linear orthogonal axes. After finding the new axis data is projected onto these axes, and one dimension is reduced. "See Fig 2.34" Problem with this approach is that if the features are essential for interpreting the data, reducing the dimension with PCA omit this information. Another problem with PCA is that reduced dimension might not present significant variance; however, it can be vital to differentiate the clusters. In some cases, applying PCA might omit this dimension. However, after working on many samples, PCA is found to be relevant, and empirical results showed that it did not reduce the performance of the FCM.

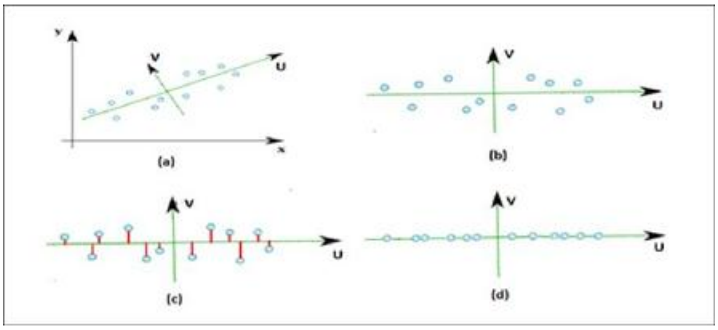

Figure 2.34 Dimension reducing process. (a) Finding the u-v axis with maximum variance. (b) Change of basis from x-y to u-v (c) projecting the data to axis with maximum variance. (d) reduced data from 2 dimensions to 1 dimension.

2.3.5 Fuzzy c means clustering

Clustering plays a vital role in segmentation and pattern recognition. In our case, cropped cross-section images needed to be divided into two clusters. The FCM algorithm is proposed by Bezdek to use in similar clustering problems. [27] Fuzzy clustering attempts to divide data into "c" groups based on their similarities and assign each sample a membership weight with a value between zero and one. In order to measure similarity, the FCM algorithm uses Euclidean distance between the feature vectors. FCM starts with random guess for cluster centers. These centers are adjusted to the right position in the data by iteratively updating the sample's membership weights and cluster centers. To update the cluster centers and membership of the samples, FCM try to optimize an objective function J_{FCM}. After reaching a stopping criterion, the algorithm stops.

$$J_{FCM} = \sum_{i=1}^{c}\sum_{j=1}^{n} (u_{ij})^m (d_{ij})^2$$

Fuzzy c means objective function. (2.15)

$u_{ij} \in [0, \infty]$is the membership weight of $x_j$in i'th cluster; $d_{ij} = \|w_i - x_j\|$ is the Euclidean distance between i'th cluster and x_j sample. C is the number of clusters; n is the number of samples. [9]. Clustering results of three different fabrics with very different appearance are shown in "See Fig 2.35"

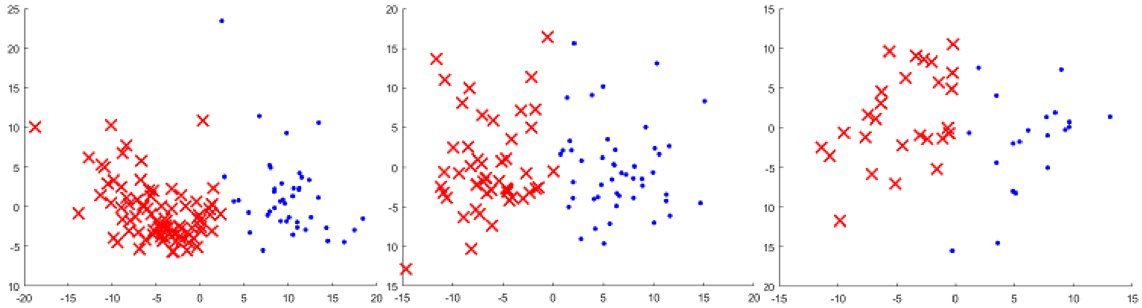

Figure 2.35 Clustering results.

For the labeling of the clusters, five samples are chosen with the highest membership weight from one cluster and asked the user to label them. The majority of the votes decide the label of the cluster. Since this is a binary clustering problem, the other cluster is automatically labeled with the other label.

CHAPTER 3 – RESULTS AND DISCUSSION

The results of the segmentation and classification process will be discussed here with statistics taken from different fabrics with different weaving structure. In general, the algorithm performs robust to detect yarn alignments for fabrics with very different types of fabrics, such as densely weaved linen to transparent crepe weaving. Detecting yarn alignments is vital for generating correct projection profiles to segment the image from the yarn boundaries. Therefore, it is convenient to state that the segmentation process is robust and working with many basic weaving patterns successfully. The part that needed to be worked on is the labeling of crossings such that whether vertical yarn goes up or down of the horizontal yarn. Although after generating GLCM features and clustering with FCM, cluster tends to accumulate the positive side of the horizontal axis for the vertical up situation for many cases, however, it is not valid for every test sample. In order to conclude, either a new feature needed to work out, such as “covariability” [33] of intensities along the horizontal or vertical direction or using a supervised algorithm such as SVM. The downside of the supervised approach is that there are many different yarn and weaving patterns, which leads to thousands of different types. Trying to come up with a supervised approach requires millions of samples. For example, three different fabric samples with different yarn types cannot be successfully classified with 600 crossing images. The validation rate was about 65 percent, which is very low.

3.1 Test results

Segmentation and classification results of three different fabric types with two samples of each given below in “table 3.1” and classification error rates given in “table 3.2”.

Table 3.1

Type1	Type2	Type 3
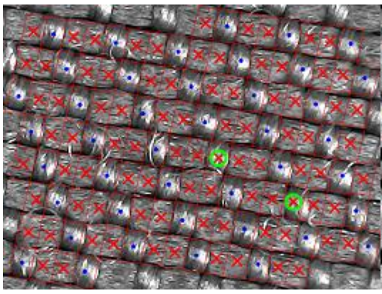	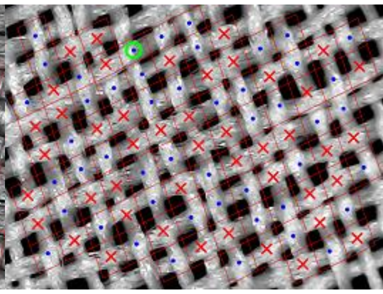	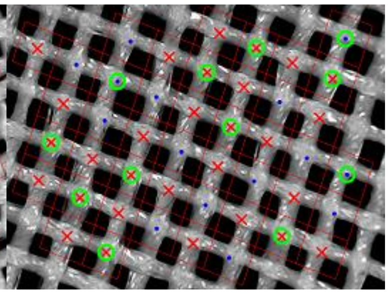
Sample 1	Sample 3	Sample 5
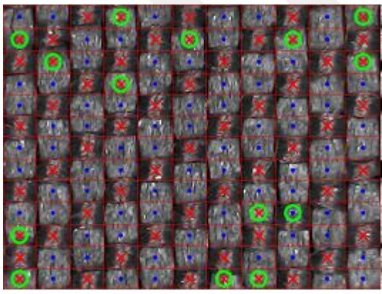	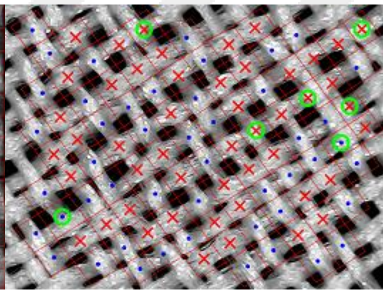	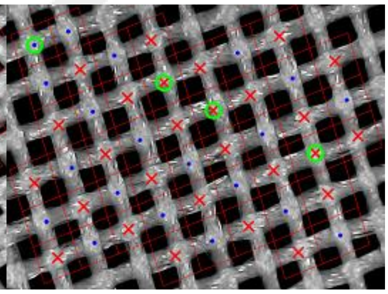
Sample 2	Sample 4	Sample 6

Table 3.2

Sample	Miss classification ratio	Error percent
1	2/128	1.56 %
2	14/143	9.79 %
3	1/93	1.07 %
4	7/97	7.21 %
5	12/44	27.27 %
6	4/47	8.51 %

Sample 5 shows a relatively high miss classification ratio, although it has a straightforward weaving pattern. This situation will be investigated further in the following section.

3.2 Critical factors related to system accuracy

One of the most critical aspects of the success of the algorithm is that captured images must be high in contrast and sharper around the edges to distinguish each yarn clearly. Unfortunately, blurred images due to low lighting, shaking camera, miss adjusted focal length produces images that show no separability between interlacing yarns. “See Fig 3.1” Another critical aspect is that the captured image must be big enough to contain multiple repetitions of the full pattern. This way smallest patch [17] can be extracted for further analyzing the weaving pattern with autocorrelation. [6]

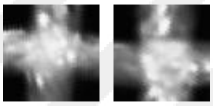

Figure 3.1 These are two samples taken from the 5’th sample. Although vertical yarn is up, it is very indistinguishable even to the human eye due to capturing problems.

3.3 Measuring system confidence

To measure both individual classifications and overall clustering performance, using the FCM membership value is a suitable approach. Because each membership value is a probability showing how likely the sample belongs to each cluster. If the membership probabilities plotted as a histogram, we expected to see a “V” shape for confident classification. The two boundary bins (0 - 1) show a high confidence level about whether the sample belongs to the first class or the other class. However, samples in the 0.5 bin show an uncertain state about the assignment of the sample. In the bad case, histogram distributes flatly or even worse; the shape increases towards the middle where the uncertainty high. Both certain and uncertain states are shown in “table 3.3”.

Table 3.3

Histogram	**Confidence**
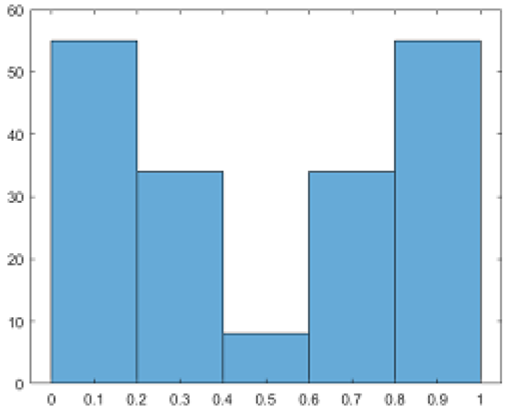	The histogram of high confident clustering taken from sample 3. The uncertain part in the middle takes low values, and boundaries are high, forming a “V“ shape.
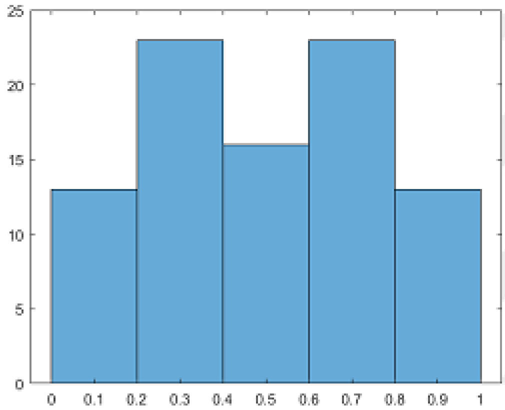	The histogram of uncertain clustering taken from sample 5. Uncertain part in the middle takes high values, and the histogram is forming a “Λ” shape.

MATLAB code for the proposed pipeline is stored in a public repository. [38].

CHAPTER 4 – CONCLUSION

A robust pipeline introduced in this thesis to segment and cluster the yarn crossing such that whether the vertical thread yarn over the horizontal yarn or the horizontal yarn passes over the vertical yarn. With this information, it is possible to construct the weaving pattern of the fabric. This information is vital to extract other parameters of the MAP model. The remaining tasks to extract parameters will be discussed here. Table 4.1 shows the parameters of the MAP model.

With this research, it can be concluded that extracting parameters of the Map model from a single photograph can be done. There will be a proposition on the possible approaches of how to extract each parameter from the segmented image in the following sub-chapters.

Table 4.1

Parameters	
η	Refraction index of the yarn.
A	Albedo color of the yarn.
k_d	Diffuse multiplier.
γ_s	Surface roughness.
γ_t	Microcylinder tangent deviation from yarn tangent.
α	Yarn ratio in the smallest patch.
Tangent Offsets	Smallest patch curve definition.
Tangent Lengths	Smallest patch curve definition.

4.1 Feature works

Parameters in table 4.1 will be extracted from the segmented image trough the proposed pipeline. The smallest patch can be extracted using autocorrelation on the weaving pattern, as discussed in this article [6] Along with this information, “Tangent Offsets” and “Tangent Lengths” can be easily extracted. After finding the smallest patch, detecting its place in the image can lead to the extraction of other parameters such as “α” ratio of each yarn in the smallest patch, “A” albedo color of each yarn. “γ_s” surface roughness “γ_t” tangent deviation of microfibers from the yarn tangent. There is another parameter, “η”

which is the refraction index of the yarn. An attempt has been made to extract this parameter, and it will be discussed in the next section.

4.2 Proposed approaches for future works

Detecting the refraction index of a transparent microfiber from a single image in our case seems not applicable therefore using a numerical approach seemed to be possible. Since the rendering equation of the MAP model can be derivate, applying the gradient descent algorithm to find a good estimation for η is a good candidate. Khungurn et al. applied a similar approach in their article "Matching Real Fabrics with Micro-Appearance Models" [28] They first constructed the same scene with the same geometric orientation, camera alignment and, lighting condition and proposed an objective function to find the difference of the rendering and the original image. Then they applied stochastic gradient descent to find the model's parameter. Analogous to their work, an image wrapped around a cylinder and lit from the front can be used in this case. The same construction can be modeled similarly in computer, and gradient descent algorithm can be applied until rendered image matches with the original image whit in an acceptable error.

5. RESOURCES

[1] Stephen R. Marschner, Henrik Wann Jensen, Mike Cammarano
"Light Scattering From Human Hair Fibers"
ACM Transactions on Graphics 22(3):780-791 · July 2003

[2] James T. Kajiya, Timothy L. Kay
"Rendering Fur With Three Dimensional Textures"
Computer Graphics, Volume 23, Number 3, July 1989

[3] Dan B. Goldman
"Fake Fur Rendering"
Conference: Proceedings of the 24th annual conference on Computer graphics and interactive techniques.
Agust 1997

[4] Tae-Yong Kim
"Modeling, Rendering And Animating Human Hair"
Faculty Of The Graduate School University Of Southern California December 2002

[5] Giuseppe Claudio Guarnera, Alain Chesnais, Mashhuda Glencross
"Woven Fabric Model Creation from a Single Image"
ACM Transactions on Graphics Volume 36 Issue 5, October 2017 Article No. 165

[6] Taewook Kang, Chang Hoon Kim, Kyung Wha Oh
"Automatic Recognition of Fabric Weave Patterns by Digital Image Analysis"
Textile Research Journal 69(2):77-83 · February 1999

[7] Kai Schröder, Arno Zinke, and Reinhard Klein
"Image-Based Reverse Engineering and Visual Prototyping of Woven Cloth"
Ieee Transactions On Visualization And Computer Graphics, Vol. 21, No. 2, February 2015

[8] J. Weickert, A. Bruhn, T. Brox, N. Papenberg
"A Survey On Variational Optic Flow Methods For Small Displacements"
Mathematical Models for Registration and Applications to Medical Imaging
Springer Berlin Heidelberg, 2006 pp. 103-136.

[9] Chung-Feng, Jeffrey Kuo, Chung-Yang, Shih, Lee, Jiunn-Yih
"Automatic Recognition of Fabric Weave Patterns by a Fuzzy C-Means Clustering Method"
Textile Research Journal; Feb 2004; 74, 2; ProQuest Central pg. 107

[10] Tomita F., Tsuji S.
"Computer Analysis of Visual Textures"
Kluwer Academic, Boston, MA, 1990 pp. 13-36.

[11] Matt Pharr, Wenzel Jakob, Greg Humphreys
Physically Based Rendering: From Theory to Implementation, Third Edition
Morgan Kaufmann; 3 edition (November 25, 2016)

[12] https://www.scratchapixel.com/lessons/mathematics-physics-for-computer-graphics/mathematics-of-shading
8 November 2019

[13] https://www.scratchapixel.com/lessons/mathematics-physics-for-computer-graphics/monte-carlo-methods-in-practice/monte-carlo-integration
5 November 2019

[14] James T. Kajiya
"The Rendering Equation"
Siggraph 1986 pp. 143-150

[15] Warren J. Smith
"Modern Optical Engineering" Third Edition
Society of Photo Optical; 3rd edition (August 1, 2000)

[16] Bui Tuong Phong
"Illumination For Computer Generated Pictures"
Communications of ACM 18 (1975), no. 6, 311–317.

[17] Iman Sadeghi, Oleg Bisker, Joachim De Deken, And Henrik Wann Jensen
"A Practical Microcylinder Appearance Model for Cloth Rendering"
ACM Transactions on Graphics Volume 32 Issue 2, April 2013 Article No. 14

[18] Hanrahan P. And Krueger W.
"Reflection from layered surfaces due to subsurface scattering"
In Proceedings of the 20th AnnualConferenceon Computer Graphics and

Interactive Techniques (SIGGRAPH’93). ACM Press, New York, 165–174.
September 1993

[19] Chandrasekhar S.
“Radiative Transfer”
Dover Publications. 1960

[20] Oge Marques
“Practical Image And Video Processing Using Matlab”
John Wiley & Sons, Inc., Hoboken, New Jersey.
July 2011

[21] R. A. Hummel
“Image Enhancement by Histogram Transformation”
Computer Graphics and Image Processing 6 (1977) 184195

[22] George Wolberg
“Digital Image Warping”
IEEE Computer Society Press, Los Alamitos, CA, USA, 1994.

[23] Namita Aggarwal, R. K. Agrawal
“First and Second Order Statistics Features for Classification of Magnetic Resonance Brain Images”
Journal of Signal and Information Processing, 2012, 3, 146-153
May 2012

[24] Robert M. Haralick
“Statistical and structural approaches to texture”
Proc. IEEE, vol. 67, no. 5, pp. 786-804, 1979.

[25] Selim Aksoy and Robert M. Haralick
“Feature Normalization and Likelihood-based Similarity Measures for Image Retrieval”
Pattern Recognition Letters - Special issue on image/video indexing and retrieval
Volume 22 Issue 5, April 2001 Pages 563 - 582

[26] Ethem Alpaydin
Introduction to Machine Learning, Third Edition
MIT Press

[27] Bezdek, J. C.
"Pattern Recognition with Fuzzy Objective Function Algorithm"
Plenum Press, NY, 1981

[28] Khungurn, P., Schroeder, D., Zhao, S., Bala, K., and Marschner, S.
"Matching Real Fabrics with Micro-Appearance Models"
ACM Transactions on Graphics .
December 2015

[29] https://www.scratchapixel.com/lessons/3d-basic-rendering/phong-shader-BRDF
8 November 2019

[30] https://www.scratchapixel.com/lessons/3d-basic-rendering/introduction-to-shading/diffuse-lambertian-shading
8 November 2019

[31] https://www.mathworks.com/help/images/ref/radon.html
8 November 2019

[32] http://murphylab.web.cmu.edu/publications/boland/boland_node26.html
8 November 2019

[33] S. Anila, K. Sheela Sobana Rani, B. Saranya
"Fabric Texture Analysis and Weave Pattern Recognition by Intelligent Processing"
Journal of Telecommunication, Electronic and Computer Engineering ISSN: 2180 – 1843 e-ISSN: 2289-8131 Vol. 10 No. 1-13.
August 2018

[34] https://www.mathworks.com/help/images/ref/graycomatrix.html
8 November 2019

[35] GLSL Implementation Of Kajiya-Kay's Hair Shader
https://github.com/afraidofdark/Thesis/blob/master/Shaders/kajiyaFrag.shader
12 November 2019

[36] GLSL implementation of Kim's hair shader.
https://github.com/afraidofdark/Thesis/blob/master/Shaders/kimFrag.shader
12 November 2019

[37] GLSL implementation of Sadeghi's MAP model.
https://github.com/afraidofdark/Thesis/blob/master/Shaders/sadegiFrag.shader
12 November 2019

[38] Proposed Image Segmentation And Clustering Pipeline In MATLAB.
https://github.com/afraidofdark/Thesis/tree/master/Matlab
12 November 2019

CV

Personal Info:

Name: Cihan Bal

Birthday: 26 - 05 -1987

Location: Turkey – İstanbul

Contact:

E-mail: cihanball@outlook.com

Education:

- (Vocational School) Computer Programing & Technologies program at Bahçeşehir University. 2007
- Bachelor's degree in computer science and engineering at Marmara University in İstanbul. 2013
- Master's degree in computer science and engineering at Marmara University in İstanbul. 2020

Summary:

I have been interested in real-time computer graphics and cad development since 2007. Therefore, I am experienced in developing software that uses system resources efficiently and high-performance applications written with C++. I am actively developing a local CAD program called ideCad.

Other Interested Fields:

- Machine Learning - Image Processing & Computer Vision.

Computer Graphics:

- Real-time Inverse Kinematics and Procedural Animation Generation.
- Real-time Lighting (Shadows and Global Illumination).
- DirectX 11 and HLSL shader programming.
- OpenGL ES 3.0 – 2.0 and GLSL shader programming.
- Procedural 3d - 2d object generation. Mesh and Curve based.

Scientific Research Topics:

- General Math, Linear Algebra, and Geometry.
- Bayesian statistics & Learning (Naive Bayes)
- Monte - Carlo simulation and integration methods.
- Image Processing.
- Neural Networks.
- Regression Models.
- Time Series Analysis.
- Frequency Domain Signal Processing with Fourier & Wavelet transforms.
- Answer Set Programming.
- Combinatorial Optimization.
- Evolutionary Algorithms.
- Machine Learning (Naive Bayes, Logistic Regression and Support Vector Machines for classification).